Higher harmonic generation in nonlinear waveguides of arbitrary cross-section

Ankit Srivastava, Ivan Bartoli, Salvatore Salamone, and Francesco Lanza di Scalea[a)]
Department of Structural Engineering, University of California, San Diego, La Jolla, California 92093

(Received 21 October 2009; revised 10 February 2010; accepted 13 February 2010)

This article concerns the generation and properties of double harmonics in nonlinear isotropic waveguides of complex cross-section. Analytical solutions of nonlinear Rayleigh–Lamb waves and rod waves have been known for some time. These solutions explain the phenomenon of cumulative double harmonic generation of guided waves. These solutions, however, are only applicable to simple geometries. This paper combines the general approach of the analytical solutions with semi-analytical finite element models to generalize the method to more complex geometries, specifically waveguides with arbitrary cross-sections. Supporting comparisons with analytical solutions are presented for simple cases. This is followed by the study of the case of a rail track. One reason for studying nonlinear guided waves in rails is the potential measurement of thermal stresses in welded rail. © *2010 Acoustical Society of America.* [DOI: 10.1121/1.3365247]

PACS number(s): 43.35.Bf, 43.35.Cg, 43.25.Dc, 43.35.Yb [YHB] Pages: 2790–2796

I. INTRODUCTION

The study of nonlinear elastic wave propagation has been of considerable interest for the last 4 decades. This, in part, is due to the fact that nonlinear parameters are, in general, more sensitive to structural defects than linear parameters.[1] Guided waves combine the sensitivity of nonlinear parameters with large inspection ranges.[2] Therefore, their application to nondestructive evaluation and structural health monitoring has drawn considerable research interest.[2–4]

Due to the mathematical complexity of the problem, studies of nonlinear elastic waves in waveguides have been limited. The nonlinear Navier equations are further complicated by geometrical constraints essential to the generation and sustenance of guided waves. Investigations pertaining to the second harmonic generation in guided Lamb waves were reported by Deng.[5–8] In these papers, the primary and secondary fields are represented by pairs of plane waves that satisfy stress-free boundary conditions on the plate's surface. The authors conclude, among other points, that antisymmetric Lamb motion is not possible at the double harmonic. Since this method was not based on modal decomposition, the formulation is complex, and furthermore, higher order nonlinearities were not addressed. de Lima and Hamilton[9] and subsequently Deng[8] analyzed the problem of nonlinear guided waves in isotropic plates by using normal mode decomposition and forced response as suggested by Auld.[10] The authors used their formulation to explain the generation of the double harmonic and the cumulative growth of the phase matched higher harmonic guided mode. Srivastava and Lanza di Scalea[11] provided the proof for the nonexistence of antisymmetric modes at the double harmonic and generalized the result to all other higher harmonics in plates. de Lima and Hamilton[12] also gave a solution for nonlinear guided waves in rods. The rod solution was shown to yield further theoretical results on existence/nonexistence of higher harmonic by Srivastava and Lanza di Scalea.[13]

The solutions discussed above are limited in their applicability to simple geometries. This paper generalizes the approach to more complex geometries, where theoretical wave solutions are either nonexistent or hard to determine. The semi-analytical finite element (SAFE) method can help handle these cases because of its ability to extract modal solutions of waveguides of arbitrary cross-section in a computationally efficient manner.[14–20] The present study shows the validation of the approach by comparing it with analytical solutions and applies it to solve the problem of nonlinear higher harmonic generation in a rail waveguide.

II. STATEMENT OF THE NONLINEAR PROBLEM

The equation of motion for nonlinear elasticity in a stress-free waveguide is given by[9] (Fig. 1)

$$(\lambda + 2\mu)\,\nabla(\nabla \cdot \mathbf{u}) - \mu\,\nabla \times (\nabla \times \mathbf{u}) + \mathbf{f} = \rho_0 \frac{\partial^2 \mathbf{u}}{\partial t^2}, \tag{1}$$

with stress-free boundary conditions

$$[\mathbf{S^L}(\mathbf{u}) - \bar{\mathbf{S}}(\mathbf{u})] \cdot \mathbf{n_r} = \mathbf{0} \quad \text{on} \quad \Gamma, \tag{2}$$

where $\mathbf{u}$ is the particle displacement, λ and μ are the Lamé constants, ρ_0 is the initial density of the body, $\mathbf{f}$ is the body force, $\mathbf{n_r}$ is the unit vector normal to the surface of the waveguide Γ, and $\mathbf{S^L}$ and $\bar{\mathbf{S}}$ are the linear and nonlinear parts of the second Piola–Kirchoff stress tensor, respectively. Energy can be written as

$$E = \phi_2 + \phi_3 + \phi_4 \cdots, \tag{3}$$

where ϕ_n corresponds to the set of terms in the energy expression which are of degree n in strain multiples. Strain can be expressed in terms of covariant differentials of displacements

$$\varepsilon_{ij} = \tfrac{1}{2}(u_{i;j} + u_{j;i} + u_{k;i}u^k_{;j}). \tag{4}$$

[a)]Author to whom correspondence should be addressed. Electronic mail: flanza@ucsd.edu

 0001-4966/2010/127(5)/2790/7/$25.00

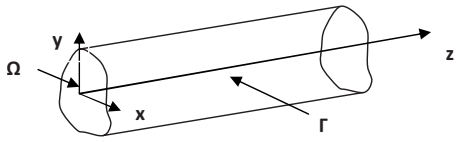

FIG. 1. Schematic of a waveguide of arbitrary cross-section.

Stress and body force are given by

$$\sigma^{ij} = \frac{\partial E}{\partial \varepsilon_{ij}}, \quad f^i = \sigma^{ij}_{;j}. \tag{5}$$

III. SOLUTION TO THE NONLINEAR PROBLEM

Following Auld[10] and de Lima and Hamilton[12] and using the method of perturbation, the first order nonlinear solution is written as linear combination of the existing guided wavemodes at 2ω as follows:

$$\mathbf{v}(\mathbf{r},z,t) = \frac{1}{2}\sum_{m=1}^{\infty} A_m(z)\mathbf{v}_m(\mathbf{r})e^{-i2\omega t} + \text{c.c.}, \tag{6}$$

where c.c. denotes complex conjugate, $\mathbf{v}_m = \partial \mathbf{u}_m / \partial t$ is the particle velocity of the mth mode at 2ω, and A_m is the higher order modal amplitude given by

$$A_m(z) = \bar{A}_m(z)e^{i(2\kappa z)} - \bar{A}_m(0)e^{i\kappa_n^* z}, \tag{7}$$

where

$$\bar{A}_m(z) = i\frac{(f_n^{\text{vol}} + f_n^{\text{surf}})}{4P_{mn}[\kappa_n^* - 2\kappa]}, \quad \kappa_n^* \neq 2\kappa \text{ (asynchronous solution)}, \tag{8}$$

$$\bar{A}_m(z) = \frac{(f_n^{\text{vol}} + f_n^{\text{surf}})}{4P_{mn}}z, \quad \kappa_n^* = 2\kappa \text{ (synchronous solution)}. \tag{9}$$

The power flow along z is

$$P_{mn} = -\frac{1}{4}\int_{\Omega} (\mathbf{v}_\mathbf{n}^* \cdot \mathbf{S}_\mathbf{m} + \mathbf{v}_\mathbf{m} \cdot \mathbf{S}_\mathbf{n}^*) \cdot \mathbf{n}_z d\Omega, \tag{10}$$

$$f_n^{\text{surf}}(z) = \int_{\Gamma} \mathbf{v}_\mathbf{n}^* \cdot \bar{\mathbf{S}} \cdot \mathbf{n}_\mathbf{r} d\Gamma, \tag{11}$$

$$f_n^{\text{vol}}(z) = \int_{\Omega} \mathbf{v}_\mathbf{n}^* \cdot \bar{\mathbf{f}} d\Omega. \tag{12}$$

Ω and Γ are the rod cross-sectional area and the rod surface, respectively (Fig. 1). κ is the wavenumber of the primary generating mode, κ_n is the wavenumber of the wave that is not orthogonal to the mth mode at the higher harmonic, and κ_n^* is its complex conjugate. $\mathbf{S}_m$ is the stress tensor for the mth mode, and $\mathbf{n}_z$ is the unit vector in the wave propagation direction z. $\bar{\mathbf{S}}$ and $\bar{\mathbf{f}}$ are the nonlinear surface traction and body force, respectively, as given by the primary wave [Eq. (5)].

IV. SEMI-ANALYTICAL FINITE ELEMENT

The SAFE method is employed to calculate the guided wave modeshapes and eigenvalues for an arbitrary cross-section which is uniform in the direction of propagation. In a nonlinear framework, the modeshapes $\mathbf{\Phi}$ are used to calculate the velocity vectors in Eq. (6), and the eigenvalues κ are the wavenumbers in the subsequent solution [Eqs. (7)–(9)]. In the SAFE method, at each frequency ω, a discrete number of guided modes is obtained. For a Cartesian reference system, the waveguide cross-section is set in the x-y plane while the z-axis is parallel to the waveguide length (see Fig. 1).

Subdividing the cross-section via finite elements, the displacement at a point $\mathbf{u}(x,y,z,t)$ in the eth element is given as

$$\mathbf{u} = \mathbf{N}\mathbf{U}^e e^{i(\kappa z - \omega t)}, \tag{13}$$

where $\mathbf{N} = \mathbf{N}(x,y)$ is the matrix of the shape functions and $\mathbf{U}^e$ is the nodal displacement vector for the eth element. The compatibility and constitutive equations can be written in synthetic matrix forms as

$$\boldsymbol{\epsilon} = \mathbf{D}\mathbf{u}, \quad \sigma = \mathbf{C}^*\boldsymbol{\epsilon}, \tag{14}$$

where $\boldsymbol{\epsilon}$ and σ are the strain and stress vectors, respectively, $\mathbf{D}$ is the compatibility operator, and $\mathbf{C}^*$ is the stiffness tensor which can be generally complex. More details on the compatibility operator can be found in Refs. 14 and 15. The principle of virtual work with the compatibility and constitutive laws, Eqs. (13) and (14), and the finite element procedure lead to

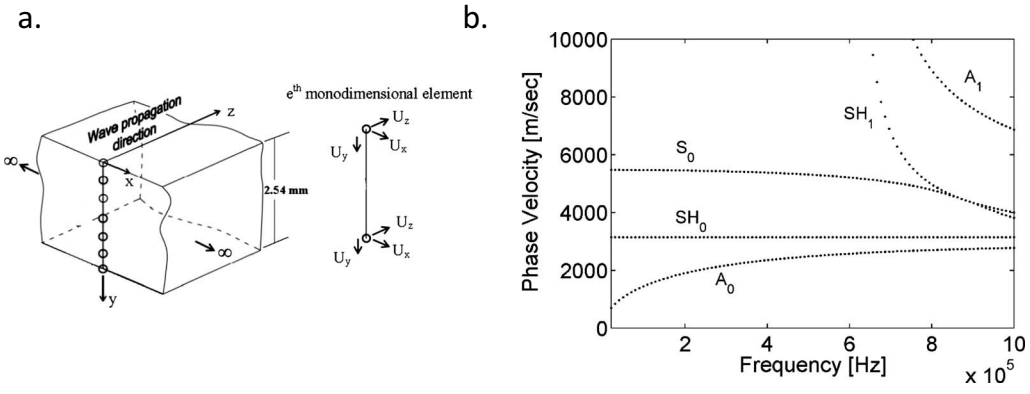

FIG. 2. (a) Schematic of the plate. (b) Phase velocity dispersion curve.

TABLE I. Material properties for the plate.

ρ_0 (kg/m^3)	c_l (m/s)	c_t (m/s)	λ [a]	μ [a]	A [a,b]	B [a,b]	C [a,b]
2727	6381	3150	57	27	−320	−200	−190

[a]In gigapascal.
[b]Third order nonlinear constants.

$$[\mathbf{A} - \kappa\mathbf{B}]_{2M}\mathbf{\Phi} = \mathbf{p}, \tag{15}$$

where the subscript $2M$ indicates the dimension of the problem with M being the number of total degrees of freedom of the cross-sectional mesh. Details on the matrices **A** and **B** can be found in Ref. 15. By setting $\mathbf{p}=0$ in Eq. (15), the associated eigenvalue problem can be solved as $\kappa(\omega)$. For each frequency ω, $2M$ complex eigenvalues, κ_m, and $2M$ complex eigenvectors $\mathbf{\Phi}_m$ are obtained. The first M components of $\mathbf{\Phi}_m$ describe the cross-sectional modeshapes of the mth mode. Once κ_m is known, phase velocity can be evaluated by the expression $c_{\text{ph}}=\omega/\kappa_{\text{real}}$, where κ_{real} is the real part of the wavenumber. The examples shown below use nondissipative materials so that $\kappa_{\text{real}}=\kappa$.

The modeshapes and wavenumbers calculated from SAFE are used in the double harmonic solution of Goldberg[21] to find the nonlinear surface and body forces $\bar{\mathbf{S}}$ and $\bar{\mathbf{f}}$, respectively. The nonlinear surface and body forces contain displacement gradients of various orders as well as second order and third order elastic constants. In these expressions, the SAFE modeshapes are needed for the cross-sectional gradients of the displacements and the SAFE wavenumbers are needed for the axial gradients of the displacements.

V. NUMERICAL SIMULATIONS

The approach of applying SAFE to nonlinear double harmonic solutions was used to solve some problems. A plate and a rod were solved first to validate the approach. Subsequently the method was applied to solve the case of higher harmonic generation in a rail cross-section. This problem cannot be solved analytically and serves to demonstrate the usefulness of the approach.

A. Plate waves

Figure 2(a) shows the geometry of the plate problem. Since the plate is infinite in x direction, derivatives with respect to x vanish and the problem reduces to plain strain. Finite element cross-sectional discretization, therefore, is done by a one-dimensional thickness discretization. Forty two-node linear elements are used. Material properties are given in Table I. Figure 2(b) shows the SAFE results for phase velocity dispersion curve for the aluminum plate between 20 kHz and 1 MHz.

It was previously shown[11] that, irrespective of the nature of the primary generating mode, antisymmetric Lamb modes cannot be generated at the double harmonic. This happens because the nonlinear power transfer from the primary mode to the secondary mode ($f_n^{\text{surf}}+f_n^{\text{vol}}$) is zero for an antisymmet-

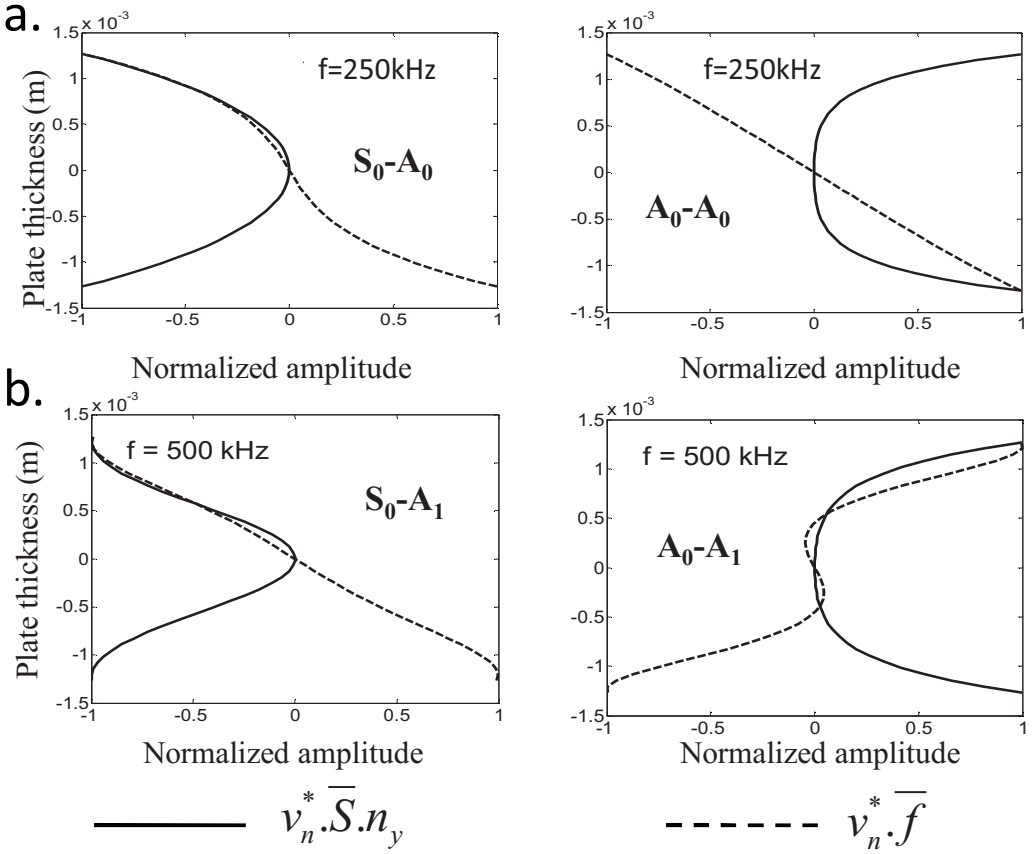

FIG. 3. Thickness profile of power flow. (a) S_0 to A_0 and A_0 to A_0 conversion. (b) S_0 to A_1 and A_0 to A_1 conversion.

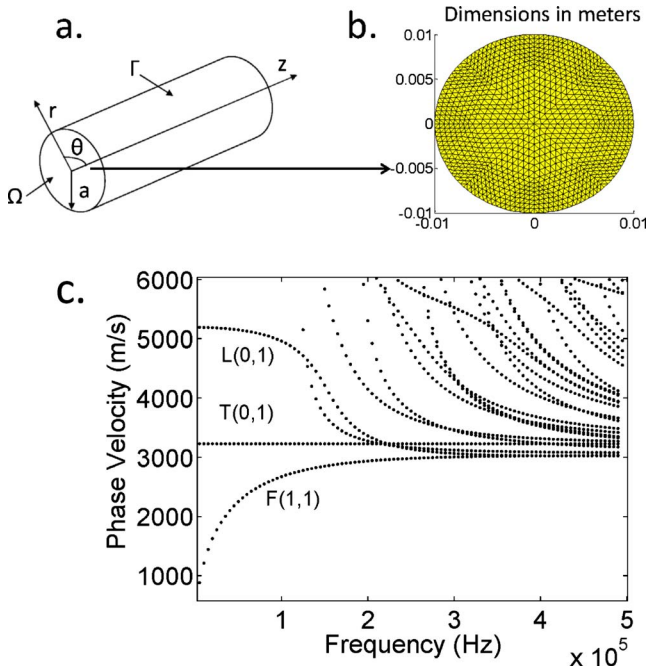

FIG. 4. (Color online) (a) Schematic of the isotropic rod. (b) Finite element discretization of the rod cross-section for SAFE analysis. (c) Phase velocity dispersion curve.

ric double harmonic mode. This, in turn, follows from the specific cross-sectional profile of the integrands in Eqs. (11) and (12). For a monodimensional discretization of a plate, the contour integral in Eq. (11) over Γ reduces to a limit value at the edges, and the surface integral in Eq. (12) over Ω reduces to a line integral over the thickness.

Figure 3 shows SAFE results for the thickness profiles of terms $\mathbf{v}_\mathbf{n}^*\cdot\bar{\mathbf{S}}\cdot\mathbf{n}_\mathbf{y}$ and $\mathbf{v}_\mathbf{n}^*\cdot\bar{\mathbf{f}}$ for modes A_0 and A_1 when the primary generating mode is S_0 and A_0, respectively. It can be seen that irrespective of the primary generating mode, $\mathbf{v}_\mathbf{n}^*\cdot\bar{\mathbf{S}}\cdot\mathbf{n}_\mathbf{y}$ is symmetric and $\mathbf{v}_\mathbf{n}^*\cdot\bar{\mathbf{f}}$ is antisymmetric across the cross-section for a potential double harmonic antisymmetric mode generation. Therefore, a contour integral of $\mathbf{v}_\mathbf{n}^*\cdot\bar{\mathbf{S}}\cdot\mathbf{n}_\mathbf{y}$ and a thickness integral of $\mathbf{v}_\mathbf{n}^*\cdot\bar{\mathbf{f}}$ reduce identically to zero. This means that there is no power transfer from any primary mode to an antisymmetric double harmonic mode implying that antisymmetric modes are absent at the double harmonic. The frequency values that refer to the primary excitation were chosen randomly. Since symmetry characteristics of these terms are not expected to change with frequency, these conclusions on the nonexistence of double harmonic flexure modes should be general. This is in accordance with theoretical predictions of Ref. 11.

TABLE II. Material properties for the rod.

ρ_0 (kg/m^3)	c_l (m/s)	c_t (m/s)	λ [a]	μ [a]	A [a,b]	B [a,b]	C [a,b]
7932	5960	3230	116.2	82.7	−320	−200	−190

[a]In gigapascal.
[b]Third order nonlinear constants.

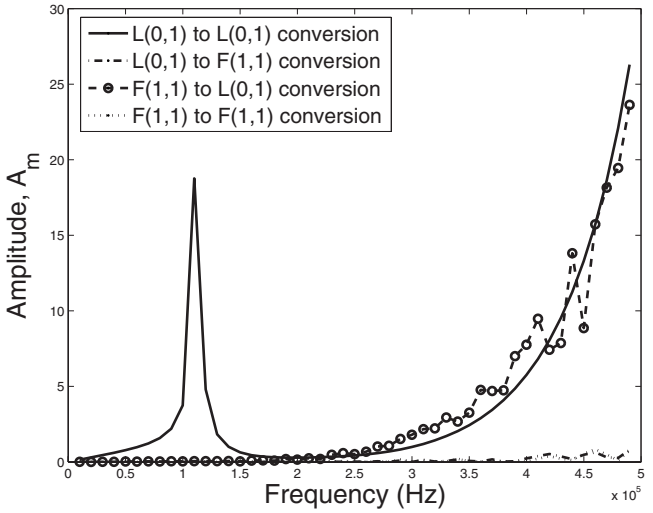

FIG. 5. Nonlinear double harmonic modal amplitudes (x values are double harmonic frequencies).

B. Rod waves

The geometry of the rod problem for SAFE is shown in Fig. 4(a). A circular cross-section of radius 0.01 m is discretized by using 512 triangular elements [Fig. 4(b)]. The material properties used in this example are given in Table II. Notice that the third order constants for this case were assumed equal to those of aluminum, which is an approximation.

Figure 4(c) shows the SAFE results for the phase velocity dispersion curve. The fundamental longitudinal $[L(0,1)]$, torsional $[T(0,1)]$, and first order flexural $(F(1,1))$ modes are marked.

de Lima and Hamilton[12] and Srivastava and Lanza di Scalea[13] have shown that the double harmonic in rod waves does not support the first order flexure mode. This happens because of the cyclic nature of sin and cos functions which makes their integrals vanish between the limits 0 and π. SAFE was used to calculate the amplitudes of the higher harmonic modes for a primary longitudinal $[L(0,1)]$ and flexural $[F(1,1)]$ generation, respectively. Figure 5 shows the variation of A_m, the double harmonic amplitude for different conversion sets as a function of frequency as computed by SAFE. The frequency vector is that of the double harmonic generation; i.e., it represents the generated modes,

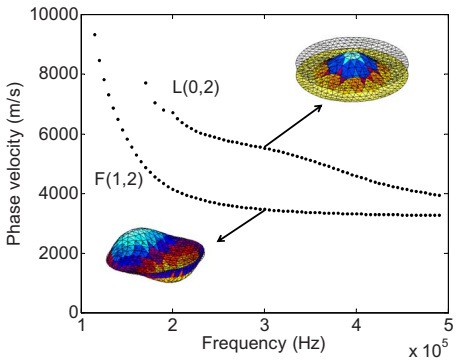

FIG. 6. (Color online) Phase velocity dispersion curve for $F(1,2)$ and $L(0,2)$ modes in the rod.

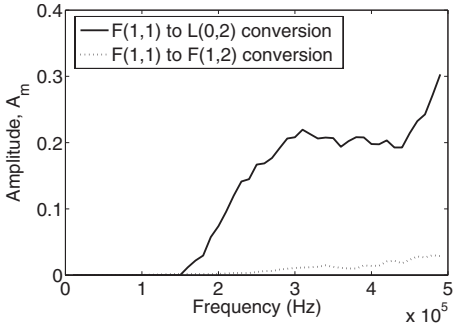

FIG. 7. Nonlinear double harmonic modal amplitudes (x values are double harmonic frequencies).

the primary generating mode being at half the frequency. The solution is in the form of an oscillating harmonic wave whose amplitude is not dependent on z.

There are several interesting points to note in the plot. The $L(0,1)$ to $L(0,1)$ conversion shows increased efficiency at two frequencies (110 and 500 kHz). The dispersion curve [Fig. 4(c)] shows that the phase velocity of the $L(0,1)$ mode is relatively nondispersive in these ranges. More specifically, the phase velocity (ω_2/κ_2) of the $L(0,1)$ mode at these frequencies is almost equal to the phase velocity (ω_1/κ_1) of the same mode at half frequencies (55 and 250 kHz). This results in phase matching where the denominator in Eq. (8) tends to zero and Eq. (9) starts becoming applicable. For the $F(1,1)$ to $L(0,1)$ conversion, a phase matching occurs at higher frequencies, and this is captured in Fig. 5 by an exponential increase in the associated A_m value above 250 kHz. Flexural mode $[F(1,1)]$ is virtually nonexistent at the double harmonic for either $L(0,1)$ or $F(1,1)$ primary excitation. Although conditions for phase matching are present for both $L(0,1)$ to $F(1,1)$ and $F(1,1)$ to $F(1,1)$ at high frequencies [Fig. 4(c)], the flexure mode is absent because there is no power transfer at the double harmonic. This is in accordance with theoretical results.

The same effect is confirmed in higher order modes. Figure 6 shows the phase velocity dispersion curve for the same rod but with two particular higher order modes extracted. The figure also shows the modeshapes of the two modes at a frequency of 300 kHz. The $F(1,2)$ mode has the same sinusoidal variation in the θ direction as the $F(1,1)$ mode. According to Srivastava and Lanza di Scalea[13] this mode would not be generated at the double harmonic. $L(0,2)$, on the other hand, has a symmetric angular variation and theory suggests that it should be likely to be generated at the nonlinear double harmonic.

Figure 7 shows the variation of A_m for $F(1,1)$ to $F(1,2)$ and $F(1,1)$ to $L(0,2)$ conversions as a function of double harmonic frequency. In line with theoretical predictions, SAFE predicts an almost zero generation of the $F(1,2)$ mode at the double harmonic. Small deviations of A_m from a value of zero at higher frequency are due to the approximations of the mesh discretization at these frequencies. The $L(0,2)$ mode, on the other hand, shows a nonzero generation at all frequencies after its cutoff. The increasing amplitude at the higher frequencies corresponds to synchronous conditions.

C. Waves in rail track

The nonlinear SAFE method was also applied to a rail. Analytical solution for the dispersion curve and the modeshapes of a rail at high frequencies are difficult to obtain. SAFE provides a good numerical tool for this problem.

Figure 8 shows a schematic of the problem along with the finite element discretization of the cross-section for SAFE analysis. A total of 470 elements were used. The material properties are same as those used in the rod example and are given in Table II.

Figure 9 shows SAFE results of the phase velocity dispersion curve for the rail cross-section under consideration.

The first few modes up to 5 kHz have been marked M_1 to M_5. Figure 9 shows the modeshapes of the modes under consideration at a frequency of 2000 Hz. The modeshapes show that M_1, M_2, M_3, and M_5 are flexure modes whereas M_4 is a longitudinal mode. The phase velocity plot also gives a rough estimate of possible phase matching synchronism that may happen between modes. In Fig. 9, there is a possibility of phase matching between M_2 and M_3 at about 3000 Hz double harmonic frequency, M_3 and M_2 at about 400 Hz double harmonic frequency, and in the M_4 to M_4 conversion at several frequencies.

Figure 10 plots the SAFE results for conversion amplitudes, A_m as calculated from Eq. (8), for the first five double harmonic modes when the primary generating mode is M_1, M_2, M_3, or M_4. It can be seen that M_1 as a primary generating mode is very inefficient [notice scale of Fig. 10(a)]. It is neither phase matched with any other mode nor does it successfully transfer power $(f_n^{\text{surf}}+f_n^{\text{vol}})$ to a higher order mode.

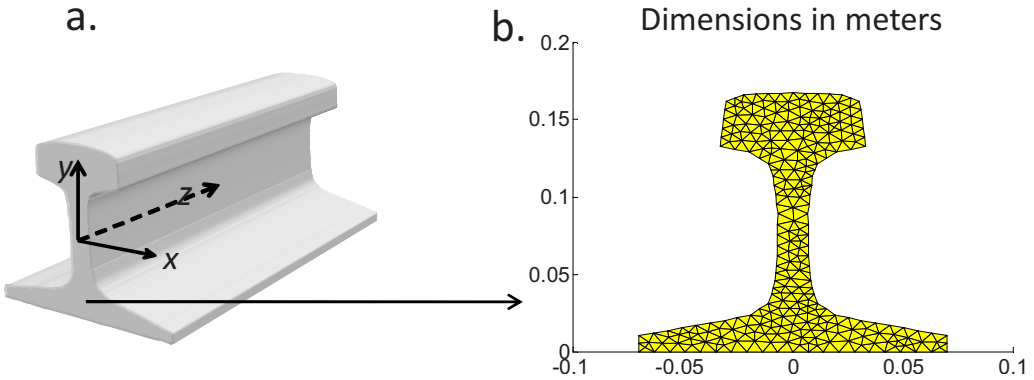

FIG. 8. (Color online) (a) Schematic of the isotropic rail. (b) Finite element discretization of the rail cross-section for SAFE analysis.

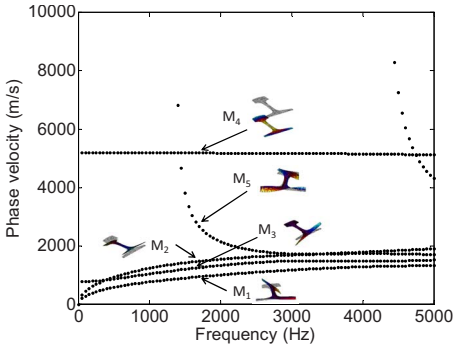

FIG. 9. (Color online) Phase velocity dispersion curve and modeshapes for the rail cross-section.

On the other hand, M_2 shows a phase matching with M_3 at a double harmonic frequency of 3600 Hz, as evident by the spike in the associated A_m value [Fig. 10(b)]. There is also a synchronization between M_3 as a generating mode and M_2 as the double harmonic mode at the double harmonic frequency of 300 Hz [Fig. 10(c)]. Another interesting point in Fig. 10(c) is the M_3 to M_4 conversion at low frequencies. There is no phase matching, as is evident from the dispersion curve of Fig. 9. This indicates that the power flux transfer from the primary M_3 mode to the secondary M_4 mode is very strong at these frequencies.

It should be noted that in cases of synchronization, Eq. (8) is no longer the valid solution. Rather, the solution is given by Eq. (9) which represents a double harmonic mode that grows linearly with distance. The summation solution of Eq. (6) includes the contribution from the phased matched modes and all other modes. While the contribution of all other modes is oscillatory and bounded,[9] the contribution from the phased matched mode grows linearly with distance. When this linearly growing contribution becomes much more than the oscillatory contribution, the solution at the double harmonic can be approximated as containing just the phase matched mode. Equation (9) is valid for distances lesser than z_1, where z_1 is the distance where the secondary nonlinear solution is no longer much smaller than the primary solution.[9]

Figure 11 shows the distance variation of the x component displacement at the left bottom node of the rail produced by the double harmonic modes. This was calculated by composing the contributions of the oscillatory modes in the wavenumber domain and performing an inverse Fourier transform to the length domain. The primary generating mode is the M_2 mode at the primary frequency of 1800 Hz. This mode has a maximum amplitude of cross-sectional displacement of 0.005 m and the amplitude of the x component of displacement produced by this mode at the left bottom node is 0.0034 m. Figure 11(a) shows the contribution of all the modes present at the double harmonic except the synchronous M_3 mode. Figure 11(b) shows the contribution the linearly growing contribution of the synchronous mode. It can be seen that the phase matched mode starts dominating the oscillatory solution at a very small distance from the source. After this distance, it is a good approximation to express the double harmonic solution as just the contribution from the synchronous M_3 mode.

VI. CONCLUSIONS

A method to study the nonlinear guided wave problem in waveguides of arbitrary cross-section is presented. This method combines the modal expansion approach with the semi-analytical finite element method. Studies supporting the method by comparing its predictions with theoretical results are presented. These include the Rayleigh–Lamb plate waves and rod waves. The method is then applied to a rail cross-section where synchronous modes are identified in a fre-

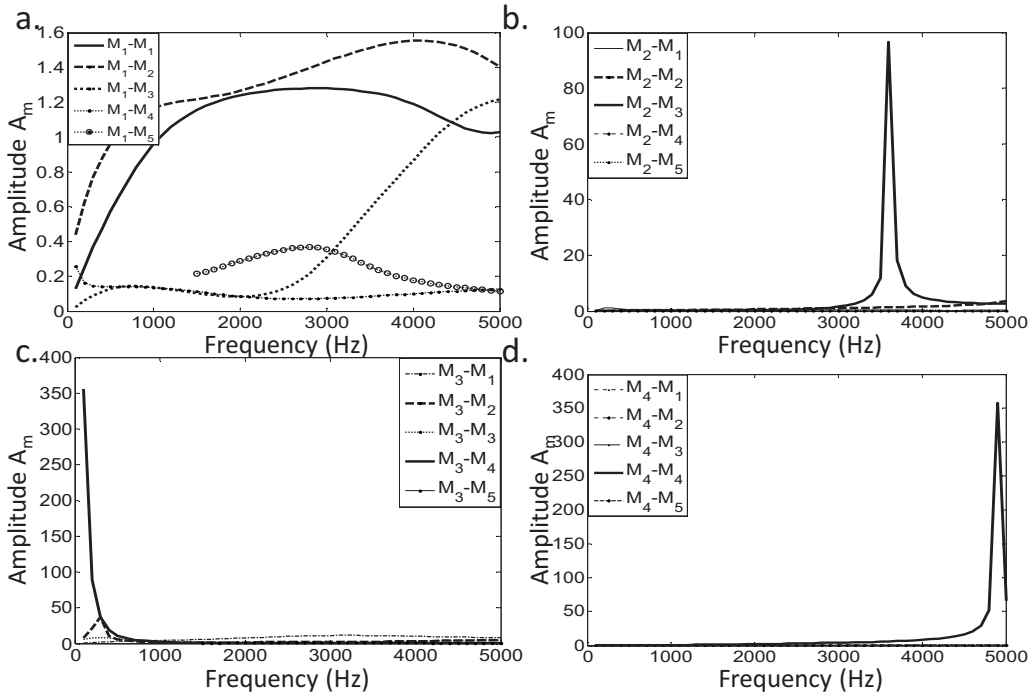

FIG. 10. Nonlinear double harmonic modal amplitudes. (a) Primary generating mode: M_1. (b) Primary generating mode: M_2. (c) Primary generating mode: M_3. (d) Primary generating mode: M_4.

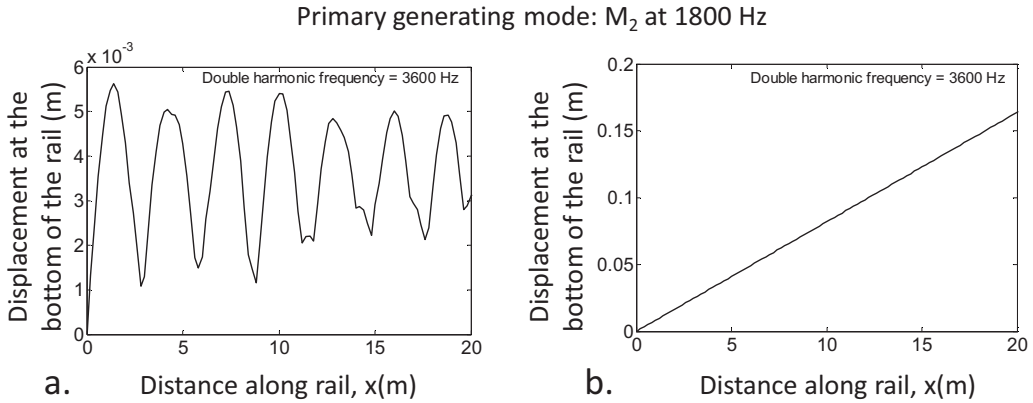

FIG. 11. x component of displacement at the left bottom node of the rail when the primary generating mode is M_2 at a frequency 1800 Hz. (a) Contribution of all double harmonic modes except the phase matched mode M_3. (b) Contribution of the phase matched mode M_3.

quency range 0–5000 Hz. The displacements contributed by all the double harmonic modes are studied and the effect of cumulative growth of the phase matched mode is shown.

ACKNOWLEDGMENTS

This work was funded by Air Force Office of Scientific Research Contract No. FA9550-07-1-0016 (Dr. V. Giurgiutiu and D. Stargel, Program Managers), Office of Naval Research Contract No. N00014-08-1-0973 (Dr. Paul Hess, Program Manager), and by the California Department of Transportation under Contract No. 59A0538 (Dr. C. Sikorsky, Program Manager).

[1]G. Dace, R. Thompson, D. Rehbein, and O. Buck, "Nonlinear acoustics, a technique to determine microstructural changes in material," Rev. Prog. Quant. Nondestr. Eval. **10B**, 1685–1692 (1991).
[2]C. Bermes, J. Kim, J. Qu, and L. Jacobs, "Experimental characterization of material nonlinearity using Lamb waves," Appl. Phys. Lett. **90**, 021901 (2007).
[3]V. Zaitsev, A. Sutin, I. Belyaeva, and V. Nazarov, "Nonlinear interaction of acoustical waves due to cracks and its possible usage for cracks detection," J. Vib. Control **1**, 335–344 (1995).
[4]A. Ekimov, I. Didenkulov, and V. Kazakov, "Modulation of torsional waves in a rod with a crack," J. Acoust. Soc. Am. **106**, 1289–1292 (1999).
[5]M. X. Deng, "Second-harmonic properties of horizontally polarized shear modes in an isotropic plate," Jpn. J. Appl. Phys., Part 1 **35**, 4004–4010 (1996).
[6]M. X. Deng, "Cumulative second-harmonic generation accompanying nonlinear shear horizontal mode propagation in a solid plate," J. Appl. Phys. **84**, 3500–3505 (1998).
[7]M. X. Deng, "Cumulative second-harmonic generation of Lamb-mode propagation in a solid plate," J. Appl. Phys. **85**, 3051–3058 (1999).
[8]M. X. Deng, "Analysis of second-harmonic generation of Lamb modes using a modal analysis approach," J. Appl. Phys. **94**, 4152–4159 (2003).
[9]W. J. N. de Lima and M. F. Hamilton, "Finite-amplitude waves in isotropic elastic plates," J. Sound Vib. **265**, 819–839 (2003).
[10]B. Auld, *Acoustic Fields and Waves in Solids* (Krieger, Malabar, Florida, 1990).
[11]A. Srivastava and F. Lanza di Scalea, "On the existence of antisymmetric or symmetric Lamb waves at nonlinear higher harmonics," J. Sound Vib. **323**, 932–943 (2009).
[12]W. J. N. de Lima and M. F. Hamilton, "Finite amplitude waves in isotropic elastic waveguides with arbitrary constant cross-sectional area," Wave Motion **41**, 1–11 (2005).
[13]A. Srivastava and F. Lanza di Scalea, "On the existence of longitudinal or flexural waves in rods at nonlinear higher harmonics," J. Sound Vib. **329**, 1499–1506 (2010).
[14]T. Hayashi, W. Song, and J. Rose, "Guided wave dispersion curves for a bar with an arbitrary cross-section, a rod and rail example," Ultrasonics **41**, 175–183 (2003).
[15]I. Bartoli, A. Marzani, and F. Lanza di Scalea, "Modeling wave propagation in damped waveguides of arbitrary cross-section," J. Sound Vib. **295**, 685–707 (2006).
[16]D. Goetschel, S. Dong, and R. Muki, "A global local finite element analysis of axisymmetric scattering of elastic waves," ASME J. Appl. Mech. **49**, 816–820 (1982).
[17]H. Taweel, S. Dong, and M. Kazic, "Wave reflection from the free end of a cylinder with an arbitrary cross-section," Int. J. Solids Struct. **37**, 1701–1726 (2000).
[18]A. Marzani, E. Viola, I. Bartoli, F. Lanza di Scalea, and P. Rizzo, "A semi-analytical finite element formulation for modeling stress wave propagation in axisymmetric damped waveguides," J. Sound Vib. **318**, 488–505 (2008).
[19]P. Loveday, "Semi-analytical finite element analysis of elastic waveguides subjected to axial loads," Ultrasonics **49**, 298–300 (2009).
[20]J. Mu and J. Rose, "Guided wave propagation and mode differentiation in hollow cylinders with viscoelastic coatings," J. Acoust. Soc. Am. **124**, 866–874 (2008).
[21]Z. Goldberg, "Interaction of plane longitudinal and transverse elastic waves," Sov. Phys. Acoust. **6**, 306–310 (1961).